Research article

Four individually druggable MET hotspots mediate HGF-driven tumor progression

Cristina Basilico,[1,2] Anna Hultberg,[3] Christophe Blanchetot,[3] Natalie de Jonge,[3] Els Festjens,[3] Valérie Hanssens,[3] Sjudry-Ilona Osepa,[3] Gitte De Boeck,[3] Alessia Mira,[1] Manuela Cazzanti,[1,2] Virginia Morello,[1,2] Torsten Dreier,[3] Michael Saunders,[3] Hans de Haard,[3] and Paolo Michieli[1,2]

[1]Laboratory of Experimental Therapy, Candiolo Cancer Institute, Candiolo, Turin, Italy. [2]Department of Oncological Sciences, University of Torino Medical School, Candiolo, Turin, Italy. [3]arGEN-X BVBA, Zwijnaarde, Belgium.

Activation of MET by HGF plays a key role in tumor progression. Using a recently developed llama platform that generates human-like immunoglobulins, we selected 68 different antibodies that compete with HGF for binding to MET. HGF-competing antibodies recognized 4 distinct hotspots localized in different MET domains. We identified 1 hotspot that coincides with the known HGF β chain binding site on blades 2–3 of the SEMA domain β-propeller. We determined that a second and a third hotspot lie within blade 5 of the SEMA domain and IPT domains 2–3, both of which are thought to bind to HGF α chain. Characterization of the fourth hotspot revealed a region across the PSI-IPT 1 domains not previously associated with HGF binding. Individual or combined targeting of these hotspots effectively interrupted HGF/MET signaling in multiple cell-based biochemical and biological assays. Selected antibodies directed against SEMA blades 2–3 and the PSI-IPT 1 region inhibited brain invasion and prolonged survival in a glioblastoma multiforme model, prevented metastatic disease following neoadjuvant therapy in a triple-negative mammary carcinoma model, and suppressed cancer cell dissemination to the liver in a *KRAS*-mutant metastatic colorectal cancer model. These results identify multiple regions of MET responsible for HGF-mediated tumor progression, unraveling the complexity of HGF-MET interaction, and provide selective molecular tools for targeting MET activity in cancer.

Introduction

Hepatocyte growth factor (HGF), also known as scatter factor, is a pleiotropic cytokine secreted by cells of mesenchymal origin that masters a characteristic biological program known as invasive growth (1). This program, essential for embryo development and tissue regeneration, is usurped by tumor cells to survive, proliferate, and disseminate into the host organism. The MET tyrosine kinase, a high-affinity receptor for HGF, is frequently activated in human cancer (2). Aberrant activation of MET occurs by different molecular mechanisms, including receptor overexpression, point mutation, and autocrine stimulation (3). MET overexpression is the most frequent dysregulation event resulting from transcriptional activation triggered by microenvironmental signals including hypoxia, oxidative stress, and mitogenic signaling (4–6). Anticancer agents such as angiogenesis inhibitors, ionizing radiations, and molecularly targeted drugs have also been shown to increase MET expression levels (7–9). Receptor upregulation results in increased sensitivity to environmental HGF, which is ubiquitous and accumulates in the extracellular matrix of tissues because of its high avidity for glycosaminoglycans (10). Increased MET expression can also be due to c-*MET* gene amplification, a genetic condition known to be associated with MET "addiction" (11). Although cancer cells harboring multiple copies of the c-*MET* gene display constitutive MET kinase activation, they retain sensitivity to the ligand (12), which
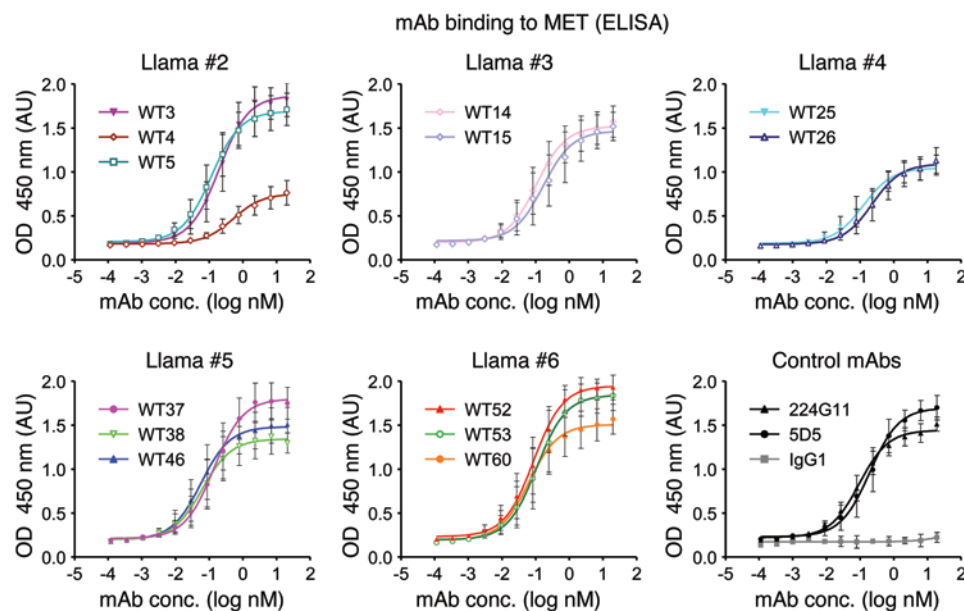
selects for c-*MET*–amplified cancer cells in a darwinian fashion (13). Point mutations in the c-*MET* gene have been reported in hereditary and sporadic papillary renal carcinoma, hepatocellular and gastric carcinoma, and head and neck cancer (14). Interestingly, mutated MET proteins require HGF stimulation in order to display their full oncogenic potential (15). Autocrine MET activation in tumors is less common, and has been reported in sarcomas, glioblastomas, and hematopoietic malignancies (16).

In spite of the importance of HGF/MET signaling in cancer biology, the mechanism by which HGF binds to and activates MET remains poorly understood. HGF is secreted as a precursor (pro-HGF) that binds to MET at high affinity but does not activate it (17). Upon proteolytic processing, pro-HGF is converted into an α-β heterodimeric ligand containing a high-affinity MET-binding site in the α chain and a low-affinity MET-binding site in the β chain (18). Cooperation between the α chain and the β chain is required for biological activity of HGF; while the α chain is sufficient for MET binding, the β chain is necessary for MET activation (19). The extracellular domain (ECD) of MET has a modular structure encompassing a 7-bladed β-propeller semaphorin homology domain (SEMA), a plexin-semaphorin-integrin homology domain (PSI), and 4 immunoglobulin-plexin-transcription factor homology domains (IPT 1–4). The β chain of active HGF binds to the "bottom" face of the β-propeller at low affinity, forming contacts with blades 2–3 (20). In contrast, high-affinity binding of the α chain of HGF to MET is more complex and less understood. Indirect experimental evidence suggests that it may interact with blade 5 of the SEMA β-propeller on one hand (21) and with the IPT region on the other (22). It is not clear whether these interactions can occur concomitantly, nor whether they are both required for HGF-induced MET activity. Failure to understand the many

Figure 1
Chimeric llama-human antibodies bind to human MET in ELISA. Binding of antibodies to MET was determined by ELISA using a purified human MET ECD protein in solid phase and increasing concentrations of the various antibodies (0–20 nM) in solution. Antibody binding was revealed using secondary anti–human Fc antibodies conjugated with HRP. An irrelevant IgG1 was used as negative control. Data related to antibodies generated by different llamas are shown in separate graphs.

faces of these complex interactions prevents the rational design of molecularly targeted drugs that interfere with HGF-mediated receptor activation and tumor progression.

In order to unmask the domains of MET responsible for interaction with HGF and to investigate their validity as therapeutic targets, we exploited a newly developed llama-based biotechnological platform that allows the production of human-like immunoglobulins. By active immunization of outbred animals (*Lama glama*) with human tumor cells expressing high levels of the MET protein, we generated a large panel of antibodies that bind to human MET at high affinity. Using this panel, we screened for antibodies that competed with HGF for binding to MET and identified a highly diverse array of antagonistic molecules. Epitope mapping using human-llama MET chimeras unveiled that these HGF-displacing antibodies recognize hotspots localized within the SEMA domain and the IPT region. Interestingly, 1 of these hotspots is located within blades 2–3 of the β-propeller and coincides with the low-affinity binding site for the HGF β chain (20). A second and a third hotspot are found within blade 5 of the β-propeller and within IPT domains 2–3, respectively, and coincide with the regions of MET where the α chain of HGF presumably binds according to indirect biochemical data (21, 22). A fourth and most represented hotspot is located across PSI and IPT 1, a region of MET not previously associated with HGF binding.

We show that antibodies directed against these hotspots inhibit HGF-induced MET activation and biological activity in biochemical and cellular assays. We also provide evidence that antibodies directed against the SEMA domain cooperate with antibodies directed against the IPT region in suppressing HGF-dependent MET activity, confirming the hypothesis that multiple sites within the MET ECD are involved in HGF interaction. By showing that these antagonistic antibodies — alone and in combination — inhibit tumor progression in HGF-dependent, orthotopic mouse models of glioblastoma multiforme, triple-negative mammary carcinoma, and metastatic colorectal cancer, we demonstrate that the hotspots identified in this study are valid targets for therapeutic intervention.

Results

Generation of HGF-competing anti-MET antibodies using a llama-based platform. In order to generate a large panel of antibodies directed against the extracellular portion of the human MET receptor in its native form, 6 llamas were immunized by intramuscular injection of 10^7 MKN-45 human gastric carcinoma cells, which display c-*MET* gene amplification and express very high levels of the MET protein (23). Animals were boosted weekly with the same amount of cells for 5 weeks (Supplemental Figure 1; supplemental material available online with this article; doi:10.1172/JCI72316DS1). Ten days after the last boost, blood samples were collected and total RNA was extracted from peripheral blood lymphocytes. The cDNAs encoding the VH-CH1 domains of llama IgG1 and the VL-CL domains (λ or κ) were amplified by PCR as described previously (24). PCR fragments were subcloned into the phagemid vector pCB3 that allows expression of recombinant antibodies as Fab fragments fused to the phage pIII envelope protein (25). Two phage libraries for each immunized animal were generated that contained a combination of immunoglobulin heavy chains with either λ- or κ-type light chains. The resulting 12 libraries were screened by panning of phages on an immobilized chimeric protein consisting of the MET ECD fused to the Fc portion of human IgG1 (MET-Fc). Two to four rounds of affinity selections were performed to enrich the libraries for phages displaying MET-specific Fabs. Individual colonies were isolated, and the Fab-containing periplasmic fraction of each individual clone was directly analyzed for its ability to compete with HGF for binding to MET in an ELISA assay (Supplemental Figure 2). Clones that scored positive in this assay were sequenced in the VH and VL regions and divided into families based on the VH CDR3 sequence. This procedure identified 68 HGF-competing Fabs belonging to 32 different VH families (Supplemental Table 1). The specificity of these clones was further characterized by surface plasmon resonance using recombinant MET ECD in solid phase and the Fabs in soluble phase. The off-rates (k_{off}) of the various clones were in the range of 10^{-3} to 10^{-4} s^{-1}.

Chimeric llama-human antibodies bind to human MET in ELISA and in living cells. From this panel of Fabs, we selected 13 clones belong-

research article

Table 1
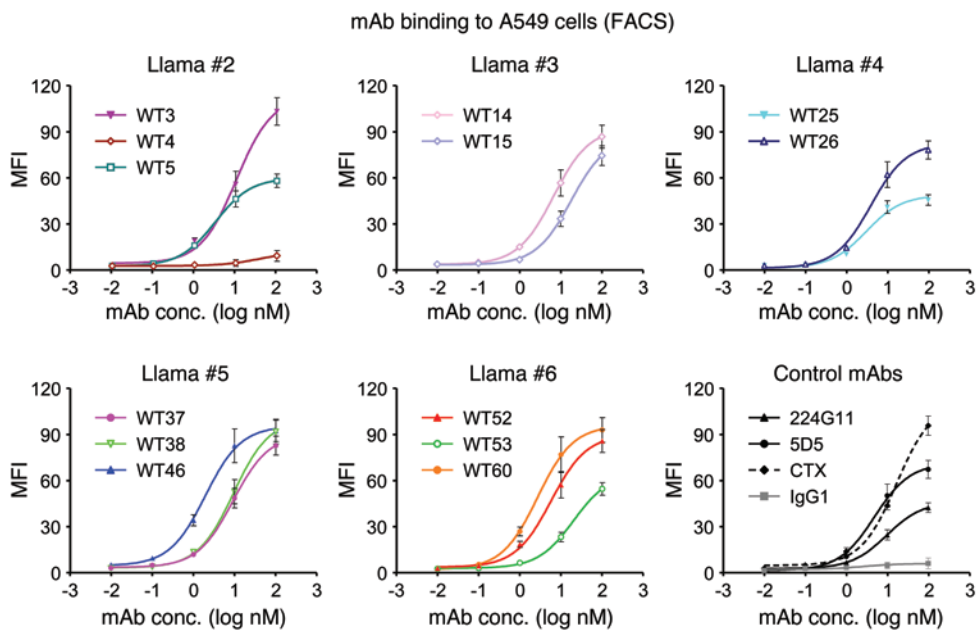Biochemical and biological properties of anti-MET antibodies

Antibody		MET binding		HGF competition		MET phosphorylation			Cell scattering	
						Antagonistic activity		Agonistic activity	Antagonistic activity	Agonistic activity
Clone	Binding domain	K_d (nM)	B_{max} (AU)	IC_{50} (nM)	E_{max} (%)	IC_{50} (nM)	E_{max} (%)	% HGF activity	Score at 200 nM	Max. score
WT3	Blades 2–3	0.2	1.9	0.6	79.2	>200	20–25	40–50	1	0–1
WT4	IPT 2–3	0.5	0.8	5.0	60.2	>200	35–45	40–50	0	0–1
WT5	Blade 5	0.1	1.7	0.2	96.4	>200	40–50	65–70	1	2–3
WT14	PSI-IPT 1	0.1	1.5	0.1	96.2	2.9	60–70	20–25	1	0–1
WT15	PSI-IPT 1	0.2	1.5	2.2	86.6	3.3	70–80	35–40	2	2–3
WT25	IPT 2–3	0.1	1.1	1.3	63.6	5.4	50–65	20–25	1	0–1
WT26	IPT 2–3	0.3	1.1	0.8	69.4	6.3	65–75	40–45	2	2–3
WT37	Blades 1–2	0.1	1.8	0.4	90.3	38.0	50–55	15–20	1	0–1
WT38	PSI-IPT 1	0.1	1.4	0.2	92.3	>200	30–35	60–65	0	0–1
WT46	PSI-IPT 1	0.1	1.5	0.1	93.6	0.7	65–75	15–20	0	0–1
WT52	Blades 2–3	0.1	2.0	0.4	90.0	0.5	70–90	10–20	0	0–1
WT53	Blades 2–3	0.1	1.9	28.1	64.2	>200	5–10	15–20	3	0–1
WT60	PSI-IPT 1	0.1	1.5	0.2	92.4	0.9	60–70	15–20	1	0–1

Binding of anti-MET antibodies to MET was tested in ELISA using MET ECD in solid phase and mAbs in solution (see Figure 1). Binding affinity (K_d) and capacity (B_{max}) were determined by nonlinear regression analysis. HGF competition was determined by ELISA using a MET-Fc chimera in solid phase and biotinylated HGF in solution (see Figure 3). E_{max} is the percent HGF displacement achieved by the highest mAb dose tested (200 nM). The ability of mAbs to inhibit HGF-induced MET phosphorylation (antagonistic activity) was analyzed using A549 cells (see Figure 6). E_{max} is the percent inhibition achieved by the highest mAb dose tested (200 nM). The ability of mAbs to promote MET phosphorylation in the absence of HGF (agonistic activity) was compared with that of recombinant HGF using A549 cells (see Supplemental Figure 6). Values correspond to percent maximal HGF activity. The ability of mAbs to inhibit HGF-induced cell scattering (antagonistic activity) was determined using HPAF-II cells (see Figure 7) and is expressed using a scoring system ranging from 0 (no scatter) to 5 (maximal scatter; see Supplemental Figure 7). The ability of mAbs to promote cell scattering in the absence of HGF (agonistic activity) was also determined in HPAF-II cells and is expressed using the same scoring system (see Supplemental Figure 8). In the whole table, single values correspond to representative experiments. When substantial experimental variability was observed, the range of variation is shown instead.

ing to 10 different VH families that displayed high HGF-displacing activity (in ELISA) and low off-rate (in surface plasmon resonance; Supplemental Figure 3A). The VH and VL regions of these Fabs were fused to human constant heavy chain domains (from IgG1) and a human constant light chain domain (κ or λ), respectively, generating chimeric llama-human mAbs (Supplemental Figure 3B). As controls, we also engineered 2 chimeric antibodies consisting of the same human constant domains fused to the murine variable regions of 5D5 (the bivalent progenitor of onartuzumab; ref. 26) and 224G11 (a humanized anti-MET antibody; ref. 27). As a negative control for binding specificity we used an irrelevant human IgG1. Chimeric antibodies were produced in a mammalian cell system, purified by protein A affinity chromatography, and tested by ELISA for their ability to bind to a purified human MET ECD (Figure 1). All antibodies tested bound to MET ECD with picomolar affinity (Table 1), displaying a K_d value ranging from 0.05 nM (WT46) to 0.52 nM (WT4). Maximum binding capacity varied from antibody to antibody, suggesting that not all the epitopes recognized by these mAbs are equally available for binding, presumably because of conformational heterogeneity of the recombinant MET ECD. ELISA binding assays using unrelated human tyrosine kinase receptors (macrophage-stimulating protein receptor, EGFR, PDGFR-α, VEGFR1), mouse MET, or llama MET unveiled that none of the 13 chimeric antibodies tested has a measurable affinity for any protein different from human MET (Supplemental Table 2). We also analyzed whether the same set of antibodies bound to MET in living cells. To this end, increasing concentrations of antibodies (0–100 nM) were incubated with A549 human lung carcinoma cells, which express physiological levels of MET (28). Antibody

binding to cells was analyzed by flow cytometry using anti–human Fc secondary antibodies. All antibodies displayed dose-dependent binding, indicating that they recognize membrane-bound MET in its native conformation (Figure 2).

Chimeric llama-human antibodies compete with HGF for binding to human MET. Next, we tested whether chimeric antibodies could compete with HGF for binding to MET in ELISA. To this end, immobilized MET-Fc was incubated with a fixed concentration of biotinylated HGF (0.3 nM) in the presence of increasing concentrations of chimeric antibodies (0–100 nM). HGF binding was revealed using streptavidin conjugated with HRP (Figure 3). Consistent with the screening strategy, this analysis revealed that all chimeric antibodies can displace HGF from MET, although with different potency and different efficacy (Table 1). In terms of potency, most antibodies achieved 50% HGF displacement at concentrations ranging from 0.07 nM (WT46) to 2.21 nM (WT15). Two antibodies were significantly less potent than the others (WT4, 4.98 nM; WT53, 28.18 nM). In terms of efficacy, only 7 antibodies (WT5, WT14, WT37, WT38, WT46, WT52, WT60) achieved more than 90% HGF displacement at the maximal dose tested. To further examine the mutual competition between anti-MET mAbs and HGF in a more biological context, we performed a mirror experiment in which A549 cells were incubated with a fixed concentration of the various antibodies (1 nM) in the presence of increasing concentrations of HGF (0–100 nM). Antibody binding was determined by flow cytometry as above. This analysis revealed that anti-MET antibody binding to cells is inversely proportional to HGF concentration (Figure 4). In contrast, HGF did not affect binding of cetuximab, an anti-EGFR antibody. Notably,

Figure 2
Chimeric llama-human antibodies bind to human MET in living cells. A549 human lung carcinoma cells, which express physiological levels of MET, were incubated with increasing concentrations of the indicated antibodies (0–100 nM). Antibody binding to cells was determined by flow cytometry using anti-human secondary antibodies conjugated with phycoerythrin. CTX, cetuximab; IgG1, irrelevant IgG1.
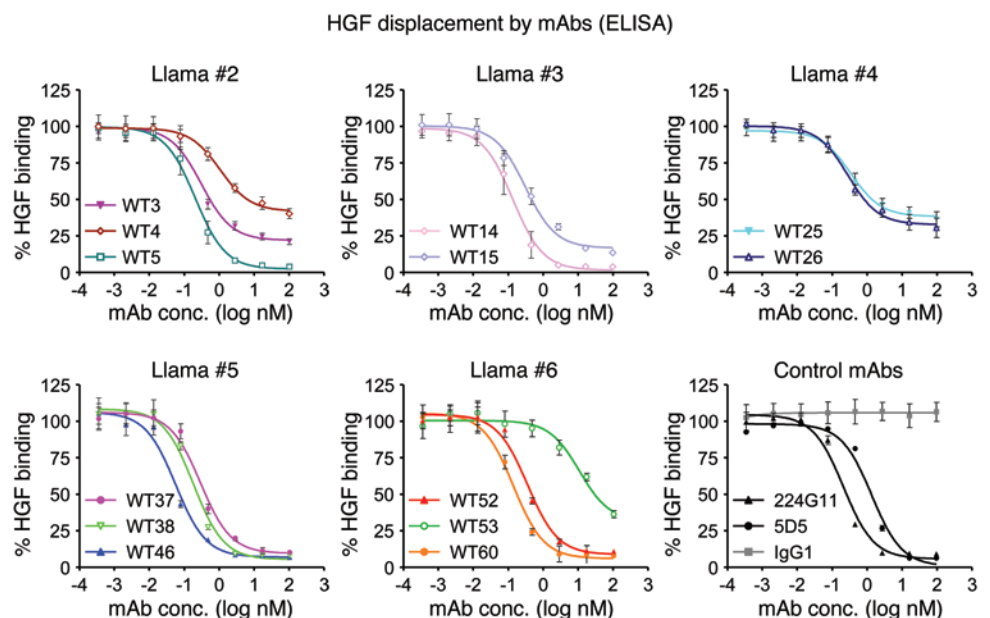
displacement of antibodies binding to MET with high affinity in both ELISA and FACS (e.g., WT38, WT46, WT52, WT60) required higher concentrations of HGF compared with other antibodies binding with lower affinity or avidity. Altogether, these results confirm that HGF and the chimeric mAbs compete for binding to the same target on living cells.

HGF-displacing mAbs recognize epitopes located throughout the MET ECD. In order to determine the epitopes recognized by HGF-competing antibodies, we measured their binding to a panel of MET engineered proteins (Supplemental Figure 4A). This panel included: the entire MET ECD (Decoy MET); a MET ECD lacking IPT domains 3 and 4 (SEMA-PSI-IPT 1–2); a MET ECD lacking IPT domains 1–4 (SEMA-PSI); the isolated SEMA domain (SEMA); and a fragment containing IPT domains 3 and 4 (IPT 3–4). ELISAs

using these engineered proteins indicated that the epitopes recognized by HGF-competing antibodies are distributed along the entire MET ECD (Supplemental Figure 4B). In fact, 5 antibodies (WT3, WT5, WT37, WT52, WT53) bound to the SEMA domain; 5 antibodies (WT14, WT15, WT38, WT46, WT60) bound within the first 2 IPT domains; and 3 antibodies (WT4, WT25, WT26) bound to Decoy MET only, suggesting that they may recognize an epitope localized between IPT domains 2 and 3. The 5D5 and the 224G11 control antibodies bound to the SEMA and the first 2 IPT domains, respectively. To more finely map these interactions, we exploited the absence of cross-reactivity between our antibodies and llama MET (Supplemental Table 2). We generated a series of llama-human and human-llama chimeric MET proteins spanning the entire MET ECD (Supplemental Figure 5). Binding of
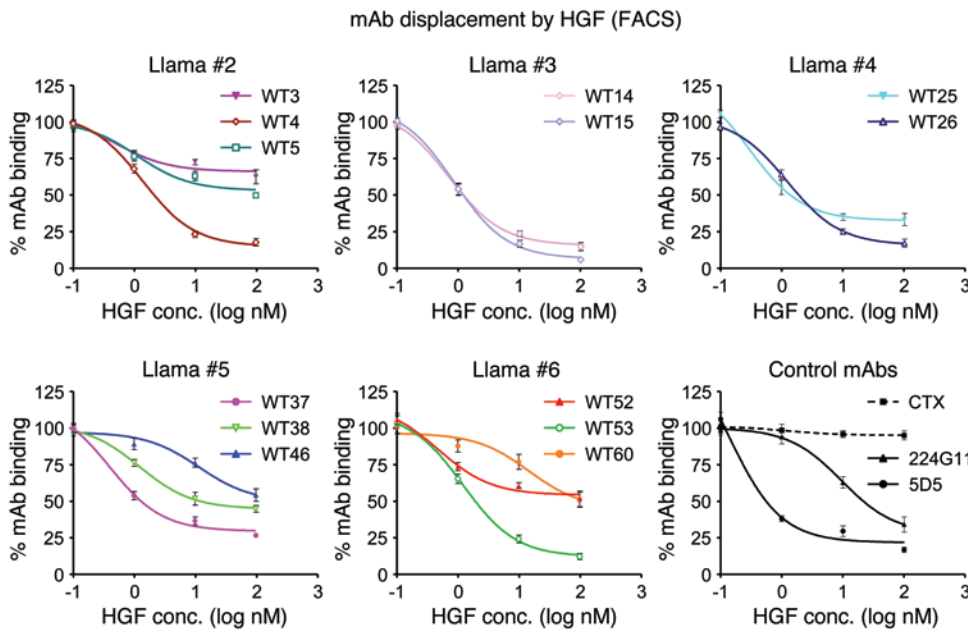
Figure 3
Chimeric llama-human antibodies antagonize HGF binding to MET in ELISA. The ability of anti-MET antibodies to compete with biotinylated HGF (0.3 nM) for binding to MET was analyzed by ELISA using MET-Fc in solid phase and increasing concentrations of chimeric antibodies (0–100 nM) in solution. HGF binding was revealed using HRP-conjugated streptavidin and expressed as percent relative to control (biotinylated HGF in the absence of mAbs). IgG1 is an irrelevant human antibody used as negative control.

mAb displacement by HGF (FACS)

Figure 4
Chimeric llama-human antibodies compete with HGF for binding onto human tumor cells. The ability of HGF to interfere with mAb binding to human tumor cells was determined by flow cytometry. A549 human lung carcinoma cells were incubated with a fixed concentration of the various antibodies (1 nM) in the presence of increasing concentrations of HGF (0–100 nM). Antibody binding to cells was determined by flow cytometry using phycoerythrin-conjugated anti-human secondary antibodies and expressed as percent relative to control (1 nM HGF in the absence of antibodies). Cetuximab (CTX) was used as a negative control.
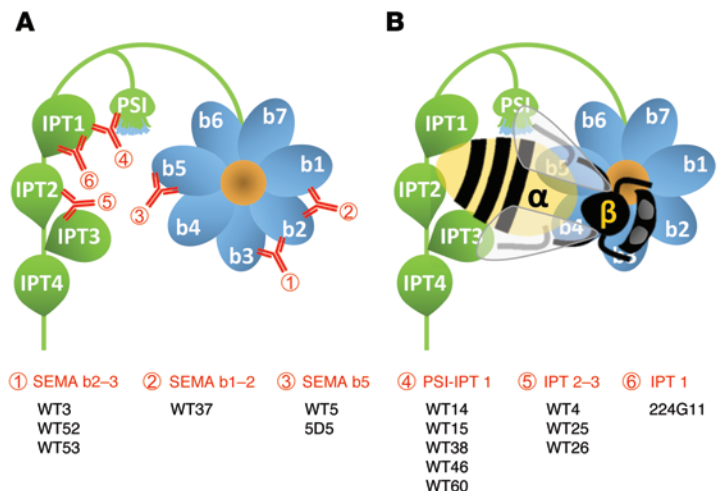
mAbs to chimeric MET was determined by ELISA. This analysis unveiled that 3 of the 5 SEMA-binding antibodies (WT3, WT52, WT53) recognize an epitope located within blades 2 and 3 (Supplemental Table 3), precisely where the β chain of HGF binds at low affinity (20). The other 2 SEMA-binding antibodies recognize an epitope located within blades 1–2 (WT37) and blade 5 (WT5). All antibodies binding to SEMA-PSI-IPT 1–2 but not to SEMA-PSI (WT14, WT15, WT38, WT46, WT60) recognize an epitope located across the PSI domain and IPT domain 1. The 3 antibodies binding to Decoy MET only (WT4, WT25, WT26) recognize an epitope located across IPT domains 2 and 3. Finally, the 5D5 and 224G11 control antibodies recognize an epitope located within blade 5 and IPT domain 1, respectively (see Figure 5A for a schematic representation). Interestingly, competition experiments revealed that antibodies directed against PSI-IPT 1 interfere with 5D5 binding to MET, and antibodies directed against blade 5 (but not blades 1–3) interfere with 224G11 binding to MET (Supplemental Table 4). The same competition pattern was observed using mAbs and
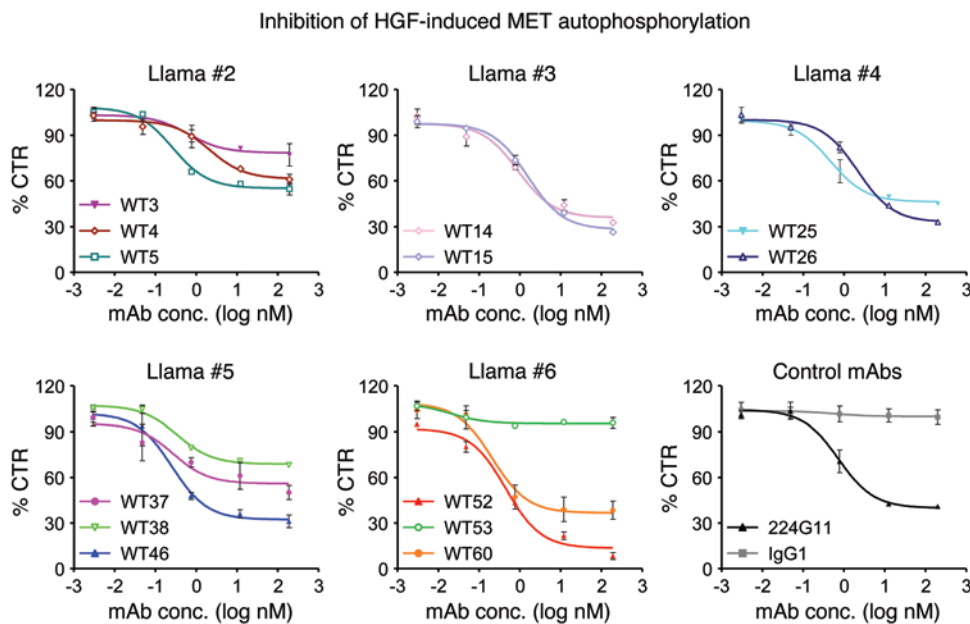
Fabs. Altogether, these results suggest a close spatial interaction between the SEMA domain and the IPT region, and are consistent with the hypothesis that HGF binds to multiple sites within the MET ECD (Figure 5B and refs. 18–22).

Chimeric llama-human anti-MET antibodies inhibit HGF-induced MET activation. The ability of HGF-competing antibodies to impair HGF-induced MET autophosphorylation was analyzed in A549 human lung carcinoma cells, which represent a standard model for studying HGF-mediated biological activity (28). Cells were incubated for 24 hours in the absence of serum and then stimulated with recombinant human HGF (1 nM) in the presence of increasing concentrations of chimeric mAbs (0–200 nM). The 224G11 antagonistic antibody and an irrelevant IgG1 were used as positive and negative control, respectively. MET autophosphorylation was determined by ELISA using phospho-MET–specific antibodies (Figure 6). This analysis revealed that 8 antibodies (WT14, WT15, WT25, WT26, WT37, WT46, WT52, WT60) strongly reduced HGF-induced MET phosphorylation, displaying

Figure 5
Schematic representation of the extracellular domain of MET and its interactions with HGF. (**A**) Representations of the hotspots identified by the HGF-competing antibodies described in this study. The corolla represents the 7-bladed β-propeller of the semaphorin homology domain (SEMA); single petals represent blades 1–7 (b1–b7). The flower bud represents the plexin-semaphorin-integrin homology domain (PSI). The leaves on the stalk represent immunoglobulin-plexin-transcription factor homology domains 1–4 (IPT 1–4). The red symbols indicate the localization of the epitopes recognized by the different antibodies. (**B**) Hypothetical model of HGF-MET interactions. The bee represents HGF, the abdomen being the α chain and the thorax and head being the β chain. The β chain interacts with SEMA blades 1–3; the α chain interacts with SEMA blade 5 on one end and with IPT 2–3 on the other. It is not clear whether the α chain interacts with PSI-IPT 1 as well or is just positioned close to them. This model is based on a synthesis of our results related to the localization of the epitopes recognized by HGF-competing antibodies with the data available in the literature (18–22).

① SEMA b2–3 ② SEMA b1–2 ③ SEMA b5 ④ PSI-IPT 1 ⑤ IPT 2–3 ⑥ IPT 1

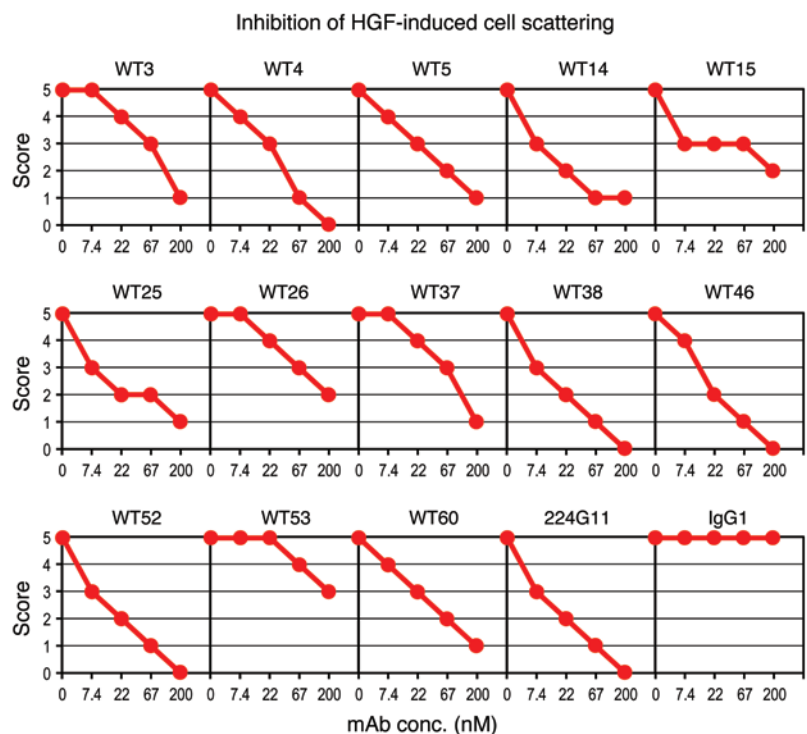| ① SEMA b2–3	② SEMA b1–2	③ SEMA b5	④ PSI-IPT 1	⑤ IPT 2–3	⑥ IPT 1
WT3	WT37	WT5	WT14	WT4	224G11
WT52		5D5	WT15	WT25	
WT53			WT38	WT26	
			WT46		
			WT60		

Figure 6
Chimeric llama-human antibodies inhibit HGF-induced MET autophosphorylation. A549 human lung carcinoma cells were stimulated with recombinant human HGF (1 nM) in the presence of increasing concentrations of chimeric mAbs (0–200 nM). The 224G11 antibody and an irrelevant IgG1 were used as positive and negative control, respectively. MET autophosphorylation was determined by ELISA using phospho-MET–specific antibodies and is expressed as percent relative to control (1 nM HGF in the absence of antibodies).

50%–90% inhibition of HGF activity at the maximal concentration tested (Table 1). Four antibodies (WT3, WT4, WT5, WT38) displayed reduced inhibitory activity (20%–50%). Consistent with its weak HGF-displacing ability (Figures 3 and 4), WT53 did not significantly inhibit HGF-induced MET autophosphorylation (5%–10%). Since the bivalent structure of antibodies can stabilize receptor dimers, thus resulting in receptor activation (29), we also investigated whether our mAbs induced HGF-independent MET autophosphorylation. To this end, we performed an analogous MET autophosphorylation assay stimulating cells with increasing concentrations (0–200 nM) of antibodies in the absence of HGF. As a positive control for MET activation we used HGF and the 5D5 antibody, which is known to display agonistic activity in its bivalent form (30). Cells were processed for ELISA as described above, and the agonistic activity of mAbs was expressed as percent maximal HGF activity (Table 1 and Supplemental Figure 6). This analysis revealed that 7 antibodies (WT14, WT25, WT37, WT46, WT52, WT53, WT60) displayed a minor agonistic effect that never exceeded 25% of maximal HGF activity at any concentration tested. Four antibodies (WT3, WT4, WT15, WT26) induced intermediate MET autophosphorylation (35%–50%), and only 2 (WT5, WT38) matched the agonistic activity of 5D5 (60%–70%).

Chimeric llama-human anti-MET antibodies inhibit HGF-induced cell scattering. To evaluate whether chimeric anti-MET antibodies could affect HGF-dependent biological activity, we tested their ability to inhibit HGF-induced cell scattering. HPAF-II human pancreatic adenocarcinoma cells (31) were stimulated with increasing concentrations of HGF (0–1.1 nM), and cell scattering was determined 20 hours later by microscopy. This preliminary analysis revealed that HGF-induced cell scattering is linear until it reaches saturation at a concentration of 0.14 nM. To quantify scatter activity, we elaborated a scoring system based on a standard HGF curve rang-

Figure 7
Chimeric llama-human antibodies inhibit HGF-induced cell scattering. HPAF-II human pancreatic adenocarcinoma cells were stimulated with 0.14 nM HGF in the presence of increasing concentrations of antibodies (0, 7.4, 22, 67, 200 nM). Scatter activity was determined 24 hours later by microscopy using a scoring system based on a standard HGF curve (0, total absence of cell scattering; 5, maximal cell scattering; see text and Supplemental Figure 7).

research article

Table 2
Concomitant targeting of the SEMA and IPT regions results in cooperative inhibition of HGF-dependent MET activity

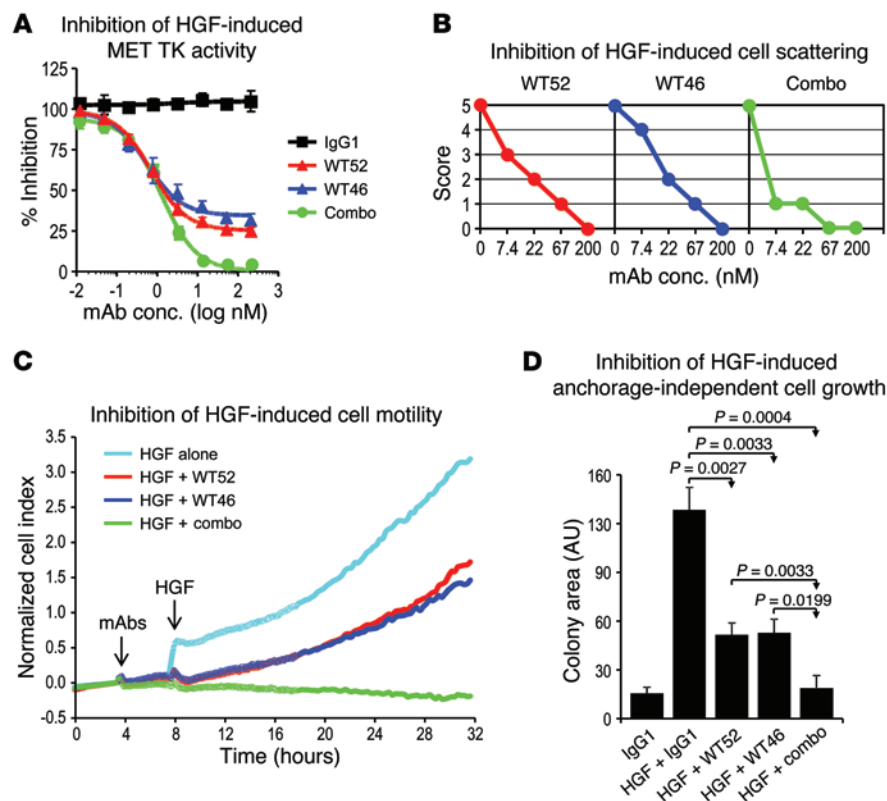| Binding domain | SEMA blade 1 | | SEMA blades 2–3 | | PSI-IPT 1 | | IPT 2–3 | |
Antibody	WT37		WT52		WT46		WT25	
Assay type	Phospho	Scatter	Phospho	Scatter	Phospho	Scatter	Phospho	Scatter
Combination with:								
WT37	54%	5	71%	3	85%[A]	4	70%[A]	4
WT52	–	–	76%	3	96%[A]	1[A]	85%[A]	4
WT46	–	–	–	–	70%	4	62%	3
WT25	–	–	–	–	–	–	57%	3

Cooperation between different antibodies was analyzed in receptor phosphorylation assays (Phospho) and cell scattering assays (Scatter). In phosphorylation assays, A549 cells were stimulated with recombinant HGF (1 nM) in the presence of increasing concentrations (0–200 nM) of single mAbs or a 1:1 mixture of 2 different mAbs. MET autophosphorylation was determined by ELISA using anti–phospho-MET antibodies. Antagonistic activity is expressed as percent inhibition at the maximal mAb dose tested (200 nM). Percent inhibition is relative to the corresponding concentration of irrelevant IgG1. In scatter assays, HPAF-II cells were stimulated with recombinant HGF (0.14 nM) in the presence of increasing concentrations (0–200 nM) of single mAbs or a 1:1 mixture of 2 different mAbs as above. Cell scattering was determined by microscopy and quantified using a scoring system ranging from 0 (no scatter) to 5 (maximal scatter). Since cooperation in scattering is manifest at low antibody concentrations, antagonistic activity is expressed as the score observed at the lowest antibody dose tested (7.4 nM) and not at the highest (200 nM) as in Table 1. Data are related to the representative experiments shown in Supplemental Figure 10 (phosphorylation) and Supplemental Figure 12 (scatter). Note that inhibition of MET tyrosine activity did not always result in inhibition of cell scattering activity (see text). [A]Values corresponding to combinations that perform better compared with both the respective single antibodies.

ing from 0 (total absence of cell scattering in the absence of HGF) to 5 (maximal cell scattering in the presence of 0.14 nM HGF; Supplemental Figure 7). We then incubated cells with 0.14 nM HGF in the presence of increasing concentrations of antibodies (0, 7.4, 22, 67, 200 nM) and determined scatter activity using the scoring system described above. The antagonistic anti-MET antibody 224G11 was used as a positive control. Results are shown in Figure 7. Four antibodies (WT4, WT38, WT46, WT52) potently inhibited HGF-induced cell scattering in a dose-dependent fashion, resulting in complete neutralization of scatter activity at the highest concentration tested (200 nM; score = 0). Six antibodies (WT3, WT5, WT14, WT25, WT37, WT60) also inhibited HGF-induced cell scattering, although they could not fully neutralize it at the highest concentration tested (200 nM; score = 1). The remaining antibodies (WT15, WT26, WT53) showed only a partial inhibitory activity. Next, we tested whether our antibodies displayed agonistic activity by inducing HGF-independent cell scattering. To this end, we stimulated HPAF-II cells with increasing concentrations of mAbs (0, 7.4, 22, 67, 200 nM) in the absence of HGF. The agonistic antibody 5D5 was used as a positive control. Scatter activity was quantified using the scoring system described above. Results are shown in Supplemental Figure 8. Only 3 mAbs (WT5, WT15, WT26) induced cell scattering to an extent comparable to 5D5. The remaining antibodies displayed no or marginal scatter activity (score = 0–1) at low concentrations but were inactive at higher doses.

Concomitant targeting of the SEMA and IPT regions results in cooperative inhibition of HGF-dependent activity. We systematically analyzed the results obtained in phosphorylation and scatter assays searching for antibodies that displayed potent antagonistic properties (maximal MET inhibition >50%; scatter score at maximal mAb concentration ≤1) and weak agonistic activity (percent HGF activity ≤25%; maximal scatter score ≤1). This analysis identified 6 antibodies binding to different MET regions (WT37 and WT52, SEMA; WT14, WT46, and WT60, PSI-IPT 1; WT25, IPT 2–3; Table 1). In order to explore a possible cooperative effect resulting from simultaneous targeting of different domains, we tested multiple antibody pairs in biochemical and biological assays. The 2 SEMA-binding mAbs recognize 2 close but distinct epitopes

located within blades 1–2 and 2–3, respectively. The 3 PSI-IPT 1–binding mAbs recognize either the same epitope or closely associated epitopes located across PSI and IPT 1. Among the latter antibodies, WT46 was selected because of its higher affinity and superior performance (Table 1). Cooperation was investigated by testing of all possible antibody pairs (WT37-WT52, WT37-WT46, WT37-WT25, WT52-WT46, WT52-WT25, WT46-WT25) in both phosphorylation and scatter experiments. In all assays, increasing concentrations (0–200 nM) of single mAbs were compared with equal concentrations of a 1:1 mixture of 2 different mAbs (i.e., 200 nM of either mAb 1 or mAb 2 is compared with 100 nM of mAb 1 + 100 nM of mAb 2). For each combination, we evaluated its ability to (a) inhibit HGF-mediated MET autophosphorylation (Supplemental Figure 9); (b) inhibit HGF-induced cell scattering (Supplemental Figure 10); (c) promote MET autophosphorylation in the absence of HGF (Supplemental Figure 11); and (d) promote cell scattering in the absence of HGF (Supplemental Figure 12). This analysis revealed that simultaneous targeting of the SEMA and IPT regions of MET resulted in enhanced inhibition of HGF-induced MET autophosphorylation (Table 2). However, only the WT52-WT46 combination resulted in a significantly improved antagonistic activity in scatter assays. No obvious advantage was achieved by any antibody combination in terms of agonistic activity, which actually appeared to increase in the WT37-WT25 and WT52-WT25 pairs. Remarkably, in both antagonism and agonism, cooperation in biochemical activity (phosphorylation) did not necessarily mirror cooperation in biological activity (scatter). This phenomenon is likely to reflect the possibility that other factors in addition to receptor tyrosine phosphorylation may also contribute to determining biological activity, including receptor internalization dynamics, duration of the signal, and differential activation of signaling pathways. Among the antibody combinations tested, the only 1 that coherently displayed a significant advantage over the corresponding single antibodies in both the assays was the WT52-WT46 pair.

The WT52 and WT46 antibodies cooperate in inhibiting HGF-mediated invasive growth. Combination of WT52 (directed against SEMA blades 2–3) and WT46 (directed against the PSI-IPT 1 domains)

Figure 8

WT52 and WT46 cooperate in inhibiting HGF-mediated invasive growth. (**A**) Inhibition of HGF-induced MET autophosphorylation. A549 cells were stimulated with 1 nM recombinant HGF in the presence of increasing concentrations (0–200 nM) of WT52, WT46, or a 1:1 mixture of WT52 and WT46 (i.e., 200 nM of either WT52 or WT46 is compared with 100 nM of WT52 + 100 nM of WT46). An irrelevant IgG1 was used as negative control. MET autophosphorylation was determined by ELISA and is expressed as percent relative to control. (**B**) Inhibition of HGF-induced cell scattering. HPAF-II cells were stimulated with 0.14 nM HGF in the presence of increasing concentrations (0–200 nM) of antibodies as in **A**. Scatter activity was determined by microscopy and is expressed using the scoring system described in the text (0, total absence of cell scattering; 5, maximal cell scattering). (**C**) Inhibition of HGF-induced cell motility. HPAF-II cells were preincubated with 200 nM WT52, 200 nM WT46, or 100 nM WT52 + 100 nM WT46 and then stimulated with 0.14 nM HGF. Cell motility was monitored in real time using an xCELLigence RTCA device and is expressed as normalized cell index. (**D**) Inhibition of HGF-induced anchorage-independent cell growth. A549 cells were grown in soft agar in the presence of 0.34 nM HGF plus 200 nM antibodies as in **C**. Colony growth was determined after 2 weeks as described in the text. Statistical significance was determined by a Student's t test ($n = 4$).

resulted in both increased efficacy and higher potency. In biochemical assays, complete inhibition of HGF-induced MET autophosphorylation was reached at a dose of 12.5 nM (6.25 nM WT52 + 6.25 nM WT46), while neither of the 2 mAbs, when used as single agents, could fully antagonize MET activation even at the highest concentration tested (Figure 8A). In biological assays, combination of WT52 and WT46 achieved a high degree of inhibition (score = 1) already at the lowest concentration tested (7.4 nM; 3.7 nM WT52 + 3.7 nM WT46), and completely suppressed HGF-induced cell scattering at a dose of 67 nM (33.5 nM + 33.5 nM; Figure 8B). Based on these results, cooperation between WT52 and WT46 was further tested in a real-time cell motility assay using an xCELLigence real time cell analyzer (RTCA). HGF-dependent HPAF-II cell motility was expressed as normalized cell index. Remarkably, while both WT52 and WT46 alone inhibited HGF-

induced motility by approximately 50%, the combination of WT52 plus WT46 achieved complete neutralization of HGF activity (Figure 8C). We also tested the WT52-WT46 combination in an anchorage-independent cell growth assay. A549 cells were seeded in soft agar in the presence of 0.34 nM HGF and treated twice weekly either with single antibodies (200 nM) or with a 1:1 antibody combination (100 nM + 100 nM). An irrelevant IgG1 was used as negative control. After 3 weeks, cell colonies were stained with tetrazolium salts, photographed, and quantified using dedicated software. In these conditions, WT52 and WT46 alone inhibited colony formation by approximately 68% and 67%, respectively, while their combination completely prevented HGF-induced anchorage-independent cell growth (Figure 8D).
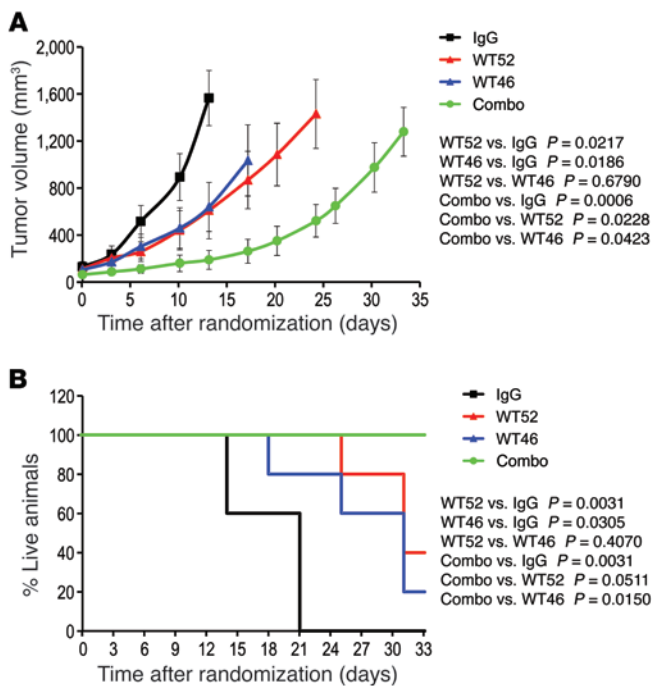
Anti-MET antibodies inhibit tumor growth in an HGF-dependent human xenograft model. Prompted by the above results, we analyzed the ability of WT52 and WT46 to interfere with HGF-dependent tumor progression in mouse models of cancer. Since mouse HGF binds to human MET with low affinity and fails to activate it (32), testing the therapeutic potential of HGF-competing antibodies in mice requires a source of human HGF. The most characterized HGF-dependent xenograft model is represented by U87-MG human glioma cells, which express both MET and HGF (30). We performed a series of preliminary experiments using different doses of WT52 and WT46 (0.3, 1, 3, 10, and 30 mg/kg) in NOD-SCID mice bearing U87-MG xenografts (Supplemental Figure 13). On the basis of this preliminary analysis, we decided to continue testing antibody activity at a dose of 10 mg/kg. To this end, U87-MG cells were injected s.c. into NOD-SCID mice. After approximately 4 weeks, mice were stratified on the basis of tumor volume and divided into 4 homogeneous groups ($n = 5$), which were randomly assigned to the following treatment arms: irrelevant IgG1 (10 mg/kg); WT52 (10 mg/kg); WT46 (10 mg/kg); and a combination of WT52 and WT46 (5 + 5 mg/kg). Antibodies were administered twice weekly by i.p. injection, and tumor growth was followed over time by caliper measurement. Mice were sacrificed when tumor volume reached 2,000 mm³. This experiment revealed that while both WT46 and WT52 significantly inhibited U87-MG xenograft growth compared with control, their combination was more effective (Figure 9A). The experiment was stopped after 5 weeks of treatment, and mouse survival was assessed by Kaplan-Meier analysis (Figure 9B). All animals in the control group had to be sacrificed before or by the third week of treatment. In contrast, by the end of the experiment, only 3 and 4 mice had been sacrificed

research article

Figure 9
Anti-MET antibodies inhibit tumor growth in an HGF-dependent human xenograft model. U87-MG human glioma cells, which express both MET and HGF, were injected s.c. into NOD-SCID mice. Mice were stratified on the basis of tumor volume and randomly assigned to 4 treatment arms (irrelevant IgG1, 10 mg/kg; WT52, 10 mg/kg; WT46, 10 mg/kg; a combination of WT52 and WT46, 5 + 5 mg/kg; $n = 5$). Antibodies were administered twice weekly by i.p. injection, and tumor growth was followed over time by caliper measurement. Mice were sacrificed when tumor volume overrode 2,000 mm^3. (**A**) Analysis of tumor volume over time. Average tumor volume was calculated for each arm until all mice in a given group were alive. Statistical significance was determined by a Student's *t* test. (**B**) Kaplan-Meier analysis of mouse survival. Statistical significance was determined using a log rank test. See also Supplemental Figure 13 for dose escalation experiments.
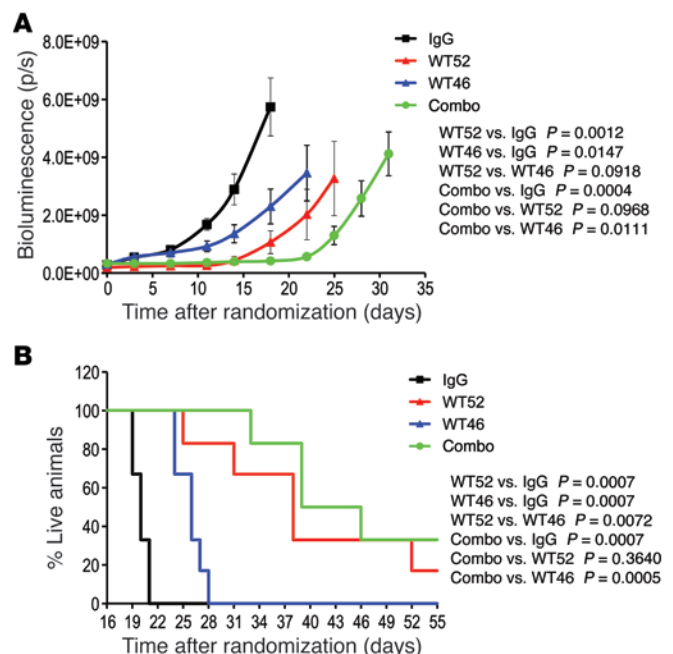
in the WT52 and WT46 groups, respectively. In the combination group, all mice survived until termination of the experiment. In a similar set of experiments aimed at assessing the in vivo specificity of antibodies, we injected NOD-SCID mice s.c. with 2 distinct human tumor cell lines not expressing MET at both the mRNA and the protein level (TOV-112D and A2780 ovarian carcinoma cells; refs. 28, 33). Tumor-bearing animals were randomized and assigned to 3 treatment arms (irrelevant IgG1, 10 mg/ml; WT52, 10 mg/ml; WT46, 10 mg/ml; $n = 6$). Antibodies were administered twice weekly by i.p. injection, and tumor volume was followed over time as above. As no statistically significant difference could be observed between any of the experimental groups tested, we conclude that the antitumor activity of WT52 and WT46 is strictly MET-dependent (Supplemental Figure 14).
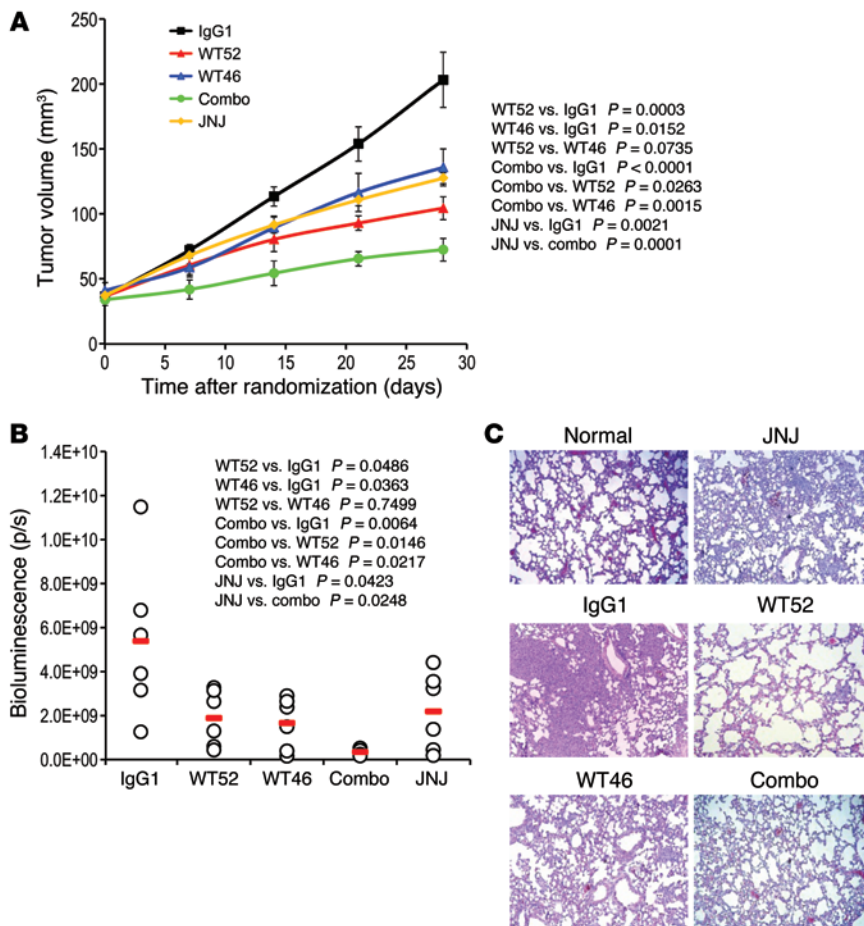
Anti-MET antibodies prolong survival in an orthotopic mouse model of glioblastoma multiforme. The pharmacological effect of WT52 and WT46 on U87-MG glioma cells was further analyzed in an orthotopic model. Luciferase-expressing U87-MG cells were microinjected into the nucleus caudatus/putamen of CD-1 nude mice using

a stereotaxic apparatus. After approximately 2 weeks, mice were stratified based on in vivo bioluminescence signal, and assigned to 4 treatment arms (IgG1, WT52, WT46, WT52 + WT46; $n = 6$). Antibodies were administered twice weekly by i.p. injection with the same dosage used in the s.c. experiment. Mice were sacrificed when showing manifest neurological symptoms, and the experiment was stopped after 8 weeks of treatment. As assessed by whole-body bioluminescence analysis, both single antibodies and their combination significantly delayed orthotopic tumor growth compared with control (Figure 10A). Kaplan-Meier analysis of experimental data revealed that all antibody treatments were associated with

Figure 10
Anti-MET antibodies prolong survival in an orthotopic mouse model of glioblastoma multiforme. U87-MG human glioma cells engineered to express luciferase were injected into the nucleus caudatus/putamen of CD-1 nude mice using a stereotaxic apparatus. Mice were stratified on the basis of in vivo bioluminescence and randomly assigned to 4 treatment arms (irrelevant IgG1, 10 mg/kg; WT52, 10 mg/kg; WT46, 10 mg/kg; a combination of WT52 and WT46, 5 + 5 mg/kg; $n = 6$). Antibodies were administered by i.p. injection twice weekly. (**A**) Tumor growth over time as assessed by whole-body bioluminescence analysis. Average tumor bioluminescence, expressed as photons per second (p/s), was calculated for each arm until all mice in a given group were alive. Statistical significance was determined by a Student's *t* test. (**B**) Kaplan-Meier analysis of mouse survival. Statistical significance was determined using a log rank test.

Figure 11

Neoadjuvant therapy with anti-MET mAbs reduces metastasis dissemination in a mouse model of orthotopic mammary carcinoma. Luciferase-expressing MDA-MB-231 human triple-negative mammary carcinoma cells were injected bilaterally into the mammary fat pad of immunodeficient NOD-SCID mice along with HGF-secreting, immortalized human mammary fibroblasts. Mice were stratified on the basis of tumor volume and randomly assigned to 5 different treatment groups (irrelevant IgG1, 10 mg/kg; WT52, 10 mg/kg; WT46, 10 mg/kg; a combination of WT52 and WT46, 5 + 5 mg/kg; JNJ-38877605, 20 mg/kg; $n = 6$). Antibodies were administered twice weekly by i.p. injection; JNJ-38877605 was administered daily by oral gavage. Tumor volume was followed over time by caliper measurement. After 4 weeks of treatment, tumors were surgically removed, and neoadjuvant therapy was interrupted. Two weeks after surgery, mice were injected with luciferin, sacrificed, and subjected to autopsy. Metastatic dissemination was determined by bioluminescence analysis of isolated organs. (**A**) Analysis of tumor volume over time. Statistical significance was calculated by a Student's t test ($n = 12$). (**B**) Bioluminescence analysis of isolated lungs at autopsy. Red bars indicate average values. Statistical significance was determined as in **A** ($n = 6$). (**C**) Representative images of lung sections stained with H&E. Original magnification, ×100. The data shown are derived from a representative experiment. An analogous experiment conducted with 5 mice per group generated overlapping results.
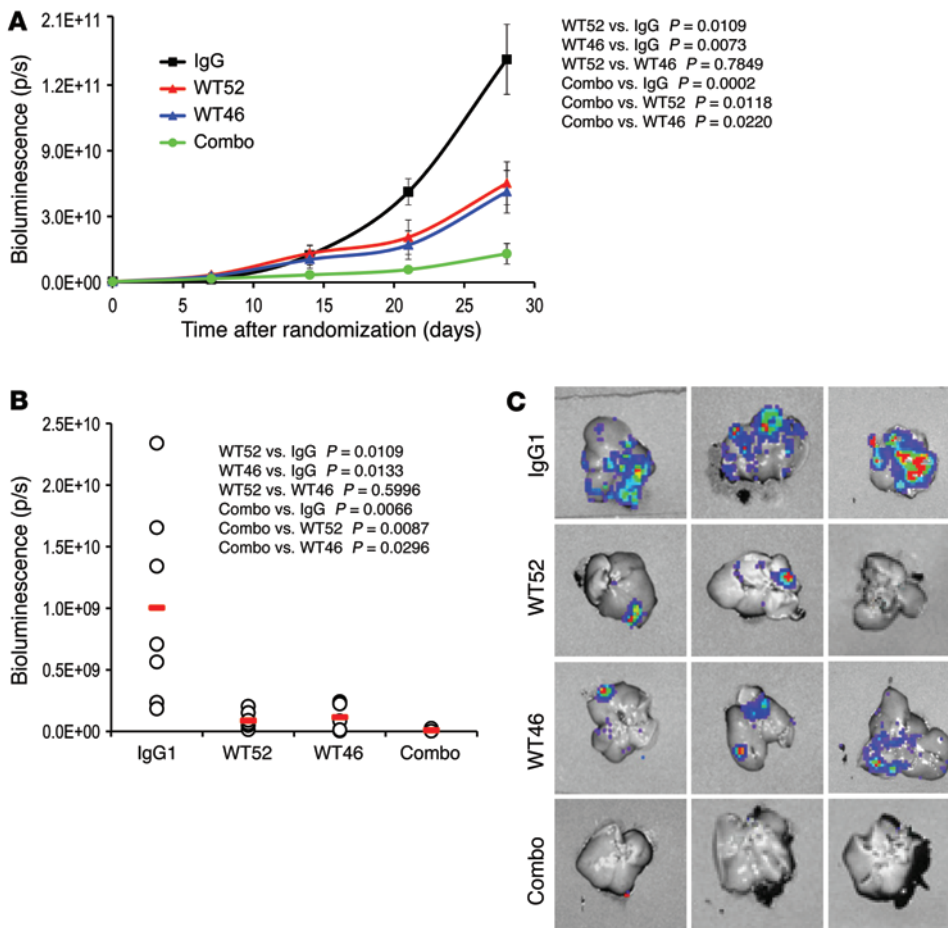
increased mouse survival (Figure 10B). However, in contrast to the s.c. setting, in which both antibodies displayed comparable activity, WT52 performed better than WT46 in this model. Consistent with this, combination of WT52 and WT46 was significantly more effective than WT46 alone, but it only showed a trend toward benefit compared with WT52. Immunohistochemical analysis of brain sections using anti–human Fc antibodies revealed comparable levels of WT52 and WT46 within the tumor, thus suggesting that this difference may not be due to increased tumor penetration by WT52 (Supplemental Figure 15A). We hypothesize that the 2 epitopes recognized by WT52 and WT46 are not equally available in the orthotopic setting, or that they play different roles in disease progression. Consistent with a role of HGF/MET signaling in glioblastoma invasion, histological analysis of brain sections revealed that all antibody-treated tumors appeared more encapsulated compared with controls and displayed a less invasive tumor-parenchyma border (Supplemental Figure 15B).

Neoadjuvant therapy with anti-MET mAbs reduces metastasis dissemination in a mouse model of orthotopic mammary carcinoma. Recent studies point at a role of HGF/MET signaling in the progression of triple-negative breast cancer (34, 35). To explore the therapeutic potential of anti-MET antibodies in this setting, we set up an orthotopic model of metastatic mammary carcinoma in which human HGF is provided paracrinally by stromal cells. Tumor growth and metastatic dissemination in this model are dependent on HGF-induced MET activation, as they can be inhibited by

anti–human HGF neutralizing antibodies (Supplemental Figure 16). Luciferase-expressing MDA-MB-231 human triple-negative mammary carcinoma cells were injected bilaterally into the mammary fat pad of immunodeficient NOD-SCID mice along with HGF-secreting, immortalized human mammary fibroblasts (36). After 2 weeks, mice were stratified on the basis of tumor volume and randomly assigned to 5 different treatment groups ($n = 6$), including the 4 antibody arms described above (IgG1, 10 mg/kg; WT52, 10 mg/kg; WT46, 10 mg/kg; WT52 + WT46, 5 + 5 mg/kg) and 1 additional arm testing a small-molecule MET tyrosine kinase inhibitor (JNJ-38877605, 20 mg/kg; refs. 37, 38). Antibodies were administered twice weekly by i.p. injection; JNJ-38877605 was administered daily by oral gavage. Tumor volume was followed over time by caliper measurement. After 4 weeks of treatment, tumors were surgically removed, and neoadjuvant therapy was interrupted. Two weeks after surgery, mice were injected with luciferin, sacrificed, and subjected to autopsy. Metastatic dissemination was determined by bioluminescence analysis of isolated lungs. This analysis revealed that both WT46 and WT52 significantly reduced tumor burden (Figure 11A) and pulmonary metastases (Figure 11B) compared with controls. Combination of the 2 antibodies was more effective than either single antibodies or JNJ-38877605 in reducing both tumor growth and metastasis, and this difference was statistically significant. Congruent results were obtained in an analogous experiment that employed 5 mice per group (not shown).

Figure 12
Anti-MET mAbs display antitumor and antimetastatic activity in an orthotopic mouse model of *KRAS*-mutant colon carcinoma. A 3:1 mix of luciferase-expressing, *KRAS*-mutant HCT-116 human colorectal carcinoma cells and HGF-secreting human colon myofibroblasts were microinjected into the cecum submucosa of NOD-SCID mice. One week after cell injection, mice were stratified on the basis of in vivo bioluminescence and randomly assigned to 4 treatment arms (irrelevant IgG1, 10 mg/kg; WT52, 10 mg/kg; WT46, 10 mg/kg; a combination of WT52 and WT46, 5 + 5 mg/kg; *n* = 7). Tumor growth was followed over time by total-body bioluminescence examination. After 4 weeks, mice were sacrificed and subjected to autopsy. (**A**) Tumor growth over time as assessed by whole-body bioluminescence. Statistical significance was calculated by a Student's *t* test. (**B**) Analysis of liver metastases as assessed by bioluminescence analysis of explanted organs. Statistical significance was calculated as in **A**. (**C**) Representative images from an independent experiment conducted in the same conditions showing luciferase signal of explanted livers.

Anti-MET mAbs display antitumor and antimetastatic activity in a KRAS-mutant orthotopic mouse model of colon carcinoma. Paracrine HGF secretion by myofibroblasts in the tumor microenvironment plays a key role in the survival, growth, and invasion of colorectal carcinoma cells (39, 40). To test whether anti-MET antibodies could interfere with this process, we set up an orthotopic model of metastatic colorectal carcinoma that resembles the environmental conditions found in human cancer (41). Briefly, luciferase-expressing human colorectal carcinoma cells are microinjected into the cecum submucosa of immunodeficient mice along with immortalized, HGF-secreting human colon myofibroblasts. Tumors in the cecum develop within a few days after cell injection and reproduce the pattern of metastatic dissemination observed in the clinic (Supplemental Figure 17A). Metastases can be conveniently detected by bioluminescence analysis of isolated organs (Supplemental Figure 17B). Myofibroblasts persist at the tumor site for the whole duration of the experiment (Supplemental Figure 17C). Experimental evidence indicates that orthotopic tumor growth and metastatic dissemination is HGF-dependent in this system (Supplemental Figure 17, D and E). To test the therapeutic potential of the WT52 and WT46 antibodies, we microinjected a 3:1 mix of luciferase-expressing, *KRAS*-mutant HCT-116 human colorectal carcinoma cells and human colon myofibroblasts into the cecum of NOD-SCID mice. One week after cell injection, mice were stratified on the basis of in vivo bioluminescence and randomly assigned to 4 treatment arms (*n* = 7) as described above

(IgG1, 10 mg/kg; WT52, 10 mg/kg; WT46, 10 mg/kg; a combination of WT52 and WT46, 5 + 5 mg/kg). Treatment continued for 4 weeks, and tumor growth was followed over time by total-body bioluminescence examination. This analysis revealed that while both antibodies significantly reduced tumor growth compared with control, their combination was significantly more effective (Figure 12A). At the end of the treatment, mice were sacrificed and subjected to autopsy. Bioluminescence analysis of liver explants revealed that both WT46 and WT52, alone or in combination, dramatically reduced metastatic dissemination compared with control (Figure 12, B and C). Combination of WT52 and WT46 reduced metastatic dissemination significantly more effectively than single antibodies. Similar results were obtained in an analogous experiment conducted independently using 5 mice per group (not shown).

Discussion
In this study we exploited a newly developed antibody platform to identify a large panel of antagonistic antibodies that compete with HGF for binding to MET. The high diversity of this panel unveiled that HGF-competing antibodies recognize epitopes clustering in several hotspots that are distributed throughout the MET ECD. This finding is consistent with the idea that the interaction between HGF and MET is very complex and involves multiple binding sites located within different domains of both the ligand and the receptor.

The hotspots identified by our HGF-competing antibodies provide useful hints for unraveling the complexity of HGF-MET interaction. The only molecularly detailed information about HGF binding to MET derives from the crystal structure of the HGF β chain in complex with the MET SEMA domain. These crystallographic data indicate that the pseudocatalytic pocket of the serine protease-like domain of HGF β chain interacts with the "bottom" face of the SEMA β-propeller, forming contacts with blades 2–3 (20). Interestingly, 1 of the hotspots identified by our antibodies (WT3, WT52, WT53) precisely coincides with this region of MET (Figure 5A), thus validating the accuracy of our system in predicting HGF-MET interactions and providing effective tools for targeting this crucial interface. A second hotspot, recognized by 1 of our antibodies (WT5) and by a control antibody (5D5), localizes within blade 5 of the SEMA β-propeller. A recent crystallographic study on onartuzumab, the 1-armed version of 5D5, confirms that this antibody forms contact with blade 5 and shows that it competes with the α chain of HGF — but not with the β chain — for binding to MET (21). Taken together, these results support a model in which HGF binds to blades 2–3 via the β chain and to blade 5 via the α chain (Figure 5B).

However, the data presented in this study suggest that this picture is not complete. In fact, our antibody-based approach identifies a third and a fourth hotspot that add complexity to the above model. The third hotspot localizes within IPT domains 2–3, a region of MET previously proposed to contain a high-affinity binding site for the α chain of HGF (22). The finding that antibodies directed against IPT domains 2–3 (WT4, WT25, WT26) compete with HGF for binding to MET supports this hypothesis and suggests that HGF α chain forms multiple interfaces with its receptor (with SEMA blade 5 on one side and with the IPT region on the other). This scenario is further complicated by the finding that the fourth and most represented hotspot is located within PSI and IPT domain 1, a region of MET not previously associated with binding to HGF. It is not clear whether antibodies binding to this hotspot displace HGF directly (by binding to the same site) or indirectly (by steric hindrance or allosteric modification). Interestingly, we observed that antibodies (mAbs or Fabs) directed against PSI-IPT 1 (WT14, WT15, WT38, WT46, WT60, 224G11) compete for binding to MET with antibodies directed against SEMA blade 5 (and vice versa), but not with antibodies directed against blades 1–3 or IPT 2–3 (Supplemental Table 3). These observations suggest that SEMA blade 5 and the PSI-IPT 1 region come in close proximity despite their distance from a primary structure viewpoint (Figure 5A). This hypothesis is consistent with the 3D data emerging from the crystal structure of the MET ECD in complex with the bacterial protein internalin B (42). Considering that all antibodies binding to any of the hotspots described here compete with HGF for binding to MET, these results support a model in which the SEMA domain and the IPT region of MET are leaned toward each other using the PSI domain as a hinge in a fashion similar to that of plexins (43) and forming a pocket into which the HGF α chain fits. In this model, the HGF β chain remains excluded from the pocket and interacts with SEMA blades 2–3, while the α chain forms contact with SEMA blade 5 on one side and with IPT domains 2–3 on the other (Figure 5B). Since there is no evidence for HGF binding directly to PSI-IPT 1 (22), we hypothesize that antibodies directed against this region of MET could recognize an allosteric epitope located across the PSI and IPT 1 domains, thus locking the pocket in a conformation that is not prone to accommodate the α chain. In support of this hypothesis,

surface plasmon resonance experiments suggest that WT46 binds at low affinity to either PSI or IPT 1, but at high affinity to PSI-IPT 1 (data not shown). Further studies are warranted to elucidate the mechanism underlying HGF α chain binding to MET.

The complexity of HGF-MET interaction unveiled by our analysis provides a rationale for explaining why simultaneous targeting of different MET domains with antagonistic antibodies achieves a cooperative effect. The results obtained in receptor autophosphorylation assays and cell scattering assays indicate that antibodies binding to the SEMA domain (blade 1 or blades 2–3) cooperate with antibodies directed against the IPT region (PSI-IPT 1 or IPT 2–3) in inhibiting HGF-induced biochemical and biological activity. However, blade 1 binders did not cooperate with blade 2–3 binders, and IPT 2–3 binders did not cooperate with PSI-IPT 1 binders (Supplemental Figures 9–12). With reference to the model proposed above, these data are congruent with the idea that HGF α chain cooperates with HGF β chain in activating MET (19) and that, in order to fully antagonize HGF activity, both these interactions must be blocked. Interestingly, the most effective cooperation was achieved combining WT52 (a blade 2–3 binder) with WT46 (a PSI-IPT 1 binder). According to the model proposed, this combination would result in displacement of HGF β chain on one hand and in conformational disruption of the α chain–harboring pocket on the other (Figure 5B). The finding that a significant fraction (5/13) of the HGF-displacing antibodies identified binds within the PSI-IPT 1 region supports the idea that this previously unidentified pocket, generated by bending of the SEMA domain over the IPT region, plays a key role in determining HGF-MET interaction and represents a strategic target for therapeutic intervention.

Although cooperation between antibodies directed against different MET domains was reproducibly observed in vitro in a variety of biochemical and biological assays, the WT52 and WT46 antibodies did not always show a sound synergistic effect in mice. This discrepancy may be due to the fact that achieving equal target engagement is not always granted in vivo. In fact, cooperation between 2 different antibodies requires both molecules to be on target at the same time at similar concentrations. This condition can be obtained without difficulty in cultured cells, but in tissues, where antibody concentration depends on a plethora of independent parameters including plasma stability, vessel permeability, drug diffusion, tissue penetration, and protein turnover, the local concentration of 2 distinct mAbs can vary significantly. Moreover, many environmental factors, including secreted cytokines, extracellular matrix components, and soluble proteases, can influence the exposure of different MET epitopes, thus preventing equal target engagement by different antibodies.

The WT52 and WT46 antibodies were selected for advanced preclinical testing not only because of their cooperation but also because each of them displayed a high antagonistic activity in conjunction with a low agonistic activity. In fact, owing to their bivalent nature, antibodies directed against the MET ECD may stabilize receptor homodimers, thus resulting in kinase activation (44). This problem can be overcome by the engineering of a monovalent immunoglobulin, like in the case of DN30 (29) and onartuzumab (30). We cannot explain why some antibodies display a more pronounced agonistic activity than others; however, thanks to the high diversity of our antibody panel targeting a variety of different MET epitopes, we had the opportunity to select HGF-competing antibodies devoid of any relevant agonistic activity, thus making protein engineering dispensable.

The preclinical results obtained with WT52 and WT46 in HGF-dependent mouse models of cancer demonstrate that the hotspots identified by these 2 antibodies are valid targets for therapy. Recent data indicate that HGF/MET signaling plays an important role in glioma cell stemness, survival, and invasion (45–47). In a mouse model of glioblastoma multiforme, in both the s.c. and orthotopic settings, WT52 and WT46 inhibited tumor growth and prolonged mouse survival. Interestingly, in the orthotopic setting, antibody-mediated inhibition of HGF/MET signaling resulted not only in reduced tumor volume (as determined by bioluminescence), but also in decreased brain parenchyma invasion, a feature characteristic of glioblastoma stem cells and a negative prognostic factor in disease progression (48).

Neoadjuvant therapy is a common clinical practice employed to reduce tumor burden before surgical intervention in invasive mammary carcinoma. Pathological complete response at the time of surgery is considered a surrogate marker of clinical benefit, and the subsequent development of clinically detectable metastases negatively impacts on overall survival. In an orthotopic mouse model of triple-negative mammary carcinoma, in which human HGF is provided paracrinally by the tumor stroma, neoadjuvant therapy with WT52 and WT46, alone or in combination, effectively reduced tumor size at the time of surgery. Most importantly, metastatic dissemination to the lung assessed 2 weeks later was dramatically decreased in the antibody arms compared with the control arm. These results point at a role of HGF-induced MET activation in sustaining breast cancer cell growth and dissemination, and warrant further exploration of HGF/MET inhibitors in the clinical management of triple-negative mammary carcinoma.

Colorectal carcinoma represents the second most frequent type of cancer worldwide, with metastatic disease being the leading cause of death. Metastatic colorectal tumors bearing mutations in the *KRAS* gene display the worst prognosis and are resistant to EGFR-targeted agents. In an orthotopic mouse model of *KRAS*-mutant colorectal cancer, in which HGF is secreted into the tumor microenvironment by human myofibroblasts, WT52 and WT46 — alone or in combination — significantly delayed primary tumor growth and, most importantly, reduced metastatic spreading to the liver, the most common metastatic site of colorectal cancer. This finding, in agreement with previous observations (49, 50), suggests that cells bearing *KRAS* mutations, although driven by KRAS signaling, take advantage of environmental HGF stimulation to invade and colonize the host organism. The possibility of inhibiting metastatic dissemination of *KRAS*-mutated cancer cells using a MET inhibitor represents an attractive therapeutic approach for an unmet medical need.

In conclusion, the data presented in this study, generated using a highly diverse panel of antagonistic antibodies, provide evidence that multiple regions of MET are responsible for interaction with its high-affinity ligand HGF, and identify several hotspots on the MET ECD as potential targets for therapy. Preclinical experiments conducted in orthotopic mouse models of cancer indicate that targeting these hotspots with antagonistic antibodies is an effective therapeutic approach to hamper tumor progression and to suppress metastatic dissemination. These findings open new translational perspectives for HGF/MET inhibitors and provide novel tools for targeting this signaling pathway in human cancer.

Methods

Llama immunization, library construction, and phage selection. Six adult llamas were immunized with a 1:1 mixture of MKN-45 human gastric carcinoma cells (10^7 cells in 1 ml of PBS; European Collection of Cell Cultures) and Freund's incomplete adjuvant (Sigma-Aldrich). Animals were boosted with the same mix every week for 5 weeks. Generation of antibody libraries was performed using the proprietary SIMPLE Antibody platform (http://www.argen-x.com/simple-antibody/). Briefly, 10 days after the last boost, 400 ml of blood was collected and PBLs were obtained using the Ficoll-Paque method (51). Total RNA was extracted as described previously (52) and used as template for random cDNA synthesis using the SuperScript III First-Strand Synthesis System kit (Life Technologies). Amplification of the cDNAs encoding the VH-CH1 regions of llama IgG1 and VL-CL domains (κ and λ) and subcloning into the phagemid vector pCB3 (Supplemental Figure 1) were performed as described previously (25). The *E. coli* strain TG1 (Netherlands Culture Collection of Bacteria) was transformed using recombinant phagemids to generate 12 different Fab-expressing phage libraries (one λ and one κ library per immunized llama). Diversity was in the range of 10^8–10^9. Fab-expressing phages were adsorbed on immobilized recombinant MET-Fc (R&D Systems) and eluted using trypsin as described previously (25). Two to four rounds of selections were performed to enrich for phages expressing MET-specific Fabs.

Fab screening and characterization. TG1 *E. coli* was infected with selected phages, and individual colonies were isolated. Secretion of Fabs was induced using IPTG (Fermentas), and the Fab-containing periplasmic fraction of bacteria was collected. Binding of Fabs to human MET was determined by ELISA using MET-Fc in solid phase and periplasmic crude extract in solution. Binding was revealed using HRP-conjugated anti-MYC antibodies (ImTec Diagnostics). Fabs that scored positive in ELISA were tested for their ability to compete with HGF for binding to MET. To this end, human MET-Fc (R&D Systems) was immobilized on ELISA plates precoated with anti–human Fc antibodies (Jackson ImmunoResearch Laboratories) and incubated with serial dilutions of Fab-containing periplasmic crude extract in the presence of 0.28 nM HGF (R&D Systems) biotinylated at the N-terminus using NHS-LC-biotin (Thermo Scientific) according to the manufacturer's instruction. Binding was revealed using HRP-conjugated streptavidin (Sigma-Aldrich). HGF-displacing Fab clones were sent out for sequencing (LGC Genomics) and divided into families based on VH CDR3 sequence length and content. VH families were given an internal number not based on International Immunogenetics Information System (IMGT) nomenclature. Binding of HGF-displacing Fabs to MET was further investigated by surface plasmon resonance using a Biacore 3000 apparatus (GE Healthcare). Human MET-Fc (R&D Systems) was immobilized on a CM-5 chip using amine coupling in sodium acetate buffer (GE Healthcare). The Fab-containing periplasmic extracts were loaded with a flow rate of 30 μl/min. The Fab off-rates (k_{off}) were measured over a 2-minute period.

Chimeric antibody production, purification, and characterization. The cDNAs encoding the VH and VL (κ or λ) domains of selected Fab fragments were engineered into 2 separate pUPE mammalian expression vectors (U-Protein Express) containing the cDNAs encoding CH1, CH2, and CH3 of human IgG1 or the human CL (κ or λ), respectively (Supplemental Figure 3B). Production (by transient transfection of mammalian cells) and purification (by protein A affinity chromatography) of the resulting chimeric llama-human IgG1 molecules was outsourced to U-Protein Express. Binding of chimeric mAbs to human MET was determined by ELISA using MET ECD in solid phase and increasing concentrations of antibodies (0–20 nM) in solution. Binding was revealed using HRP-conjugated anti–human Fc antibodies (Jackson ImmunoResearch Laboratories). The ability of chimeric mAbs to compete with HGF for binding to MET was analyzed by ELISA. MET-Fc (R&D Systems) was immobilized on ELISA plates precoated with anti-His antibodies (AbD Serotec) and incubated with 0.3 nM HGF (R&D Systems) biotinylated as described above in the presence of increasing concentrations (0–100 nM) of mAbs. Binding was revealed using HRP-conjugated strep-

tavidin (Sigma-Aldrich). Binding of chimeric mAbs to A549 human lung carcinoma cells was analyzed by flow cytometry using a CyAn ADP Analyzer (Beckman Coulter). A549 cells were incubated on ice for 30 minutes with increasing concentrations (0–100 nM) of mAbs. Binding was revealed using phycoerythrin-conjugated anti–human IgG1 antibodies (eBioscience). The ability of HGF to compete with mAbs for binding to A549 cells was determined by flow cytometry. A549 cells were incubated with 1 nM of each mAb in the presence of increasing concentrations (1–100 nM) of HGF (R&D Systems). Antibody binding was revealed using phycoerythrin-conjugated anti–human IgG1 antibodies as above. Cetuximab (Erbitux; Merck-Serono) was obtained from our clinical pharmacy.

Engineered MET proteins and epitope mapping. Deleted human MET proteins (Supplemental Figure 4) and llama-human MET chimeras (Supplemental Figure 5) were generated by standard PCR and genetic engineering techniques. All deleted MET proteins conserve the leader peptide of human MET (GenBank X54559) at their N-terminus. Their amino acid (aa) sequence corresponds to aa 1–24 (leader peptide) followed by: Decoy MET, aa 25–932; SEMA, aa 25–515; SEMA-PSI, aa 25–562; SEMA-PSI-IPT 1–2, aa 25–742; IPT 3–4, aa 743–932. Llama-human MET chimeras LS1–LS5 are composed of a llama MET portion (GenBank KF042853) at the N-terminus followed by a human MET portion at the C-terminus. Their exact amino acid sequence is described in Supplemental Figure 5. Human-llama MET chimeras LP6, LP7, and LI8–14 are composed of a human MET portion at the N-terminus followed by a llama MET portion at the C-terminus. Their exact amino acid sequence is described in Supplemental Figure 5. Binding of chimeric mAbs to deleted MET proteins and llama-human chimeras was analyzed by ELISA using engineered MET in solid phase and increasing concentrations (0–100 nM) of antibodies in solution. Binding was revealed using HRP-conjugated anti–human Fc antibodies (Jackson ImmunoResearch Laboratories). Competition between chimeric llama-human antibodies and control antibodies (5D5, 224G11) was determined by ELISA using 5D5 and 224G11 biotinylated as described above for HGF. MET-Fc (R&D Systems) was adsorbed in solid phase and incubated with a fixed concentration (1 nM) of either biotin-5D5 or biotin-224G11 in the presence of increasing concentrations (0–200 nM) of chimeric antibodies. Binding was revealed using HRP-conjugated streptavidin (Sigma-Aldrich). The same procedure was followed to analyze competition of Fabs.

Statistics. Data related to binding, displacement, and autophosphorylation were analyzed and fit using Prism software (GraphPad). Bioluminescence signal was analyzed using Living Image software (PerkinElmer). Statistical significance was determined using a log rank test (for survival) or a 2-tailed homoscedastic Student's *t* test (in all other cases). A *P* value of less than 0.05 was considered statistically significant. In all figures, values are expressed as mean and error bars represent SEM.

Study approval. All llamas used in this study were farmed outdoors in the Ardèche region of France according to the French animal welfare legislation. Animal handling was limited to immunization by i.m. injection and peripheral blood collection. Experiments involving mice were conducted in the animal facility of the Candiolo Cancer Institute – FPO, IRCCS (Candiolo, Italy). All protocols were approved by the Fondazione Piemontese per la Ricerca sul Cancro ONLUS animal research ethical committee and by the Italian Ministry of Health according to Italian legislative guidelines (Decreto Legislativo n. 116 27/01/1992 and subsequent amendments).

Supplemental Methods. For all methods not listed here, please refer to the online Supplemental Methods section.

Address correspondence to: Paolo Michieli, Candiolo Cancer Institute, Laboratory of Experimental Therapy, Strada Provinciale 142, km 3.95, I-10060 Candiolo (Torino), Italy. Phone: 39.011.9933219; Fax: 39.011.9933225; E-mail: paolo.michieli@ircc.it.

1. Boccaccio C, Comoglio PM. Invasive growth: a MET-driven genetic programme for cancer and stem cells. *Nat Rev Cancer*. 2006;6(8):637–645.
2. Birchmeier C, Birchmeier W, Gherardi E, Vande Woude GF. Met, metastasis, motility and more. *Nat Rev Mol Cell Biol*. 2003;4(12):915–925.
3. Comoglio PM, Giordano S, Trusolino L. Drug development of MET inhibitors: targeting oncogene addiction and expedience. *Nat Rev Drug Discov*. 2008;7(6):504–516.
4. Pennacchietti S, Michieli P, Galluzzo M, Mazzone M, Giordano S, Comoglio PM. Hypoxia promotes invasive growth by transcriptional activation of the met protooncogene. *Cancer Cell*. 2003;3(4):347–361.
5. Steffan JJ, Coleman DT, Cardelli JA. The HGF-met signaling axis: emerging themes and targets of inhibition. *Curr Protein Pept Sci*. 2011;12(1):12–22.
6. Seol DW, Chen Q, Zarnegar R. Transcriptional activation of the hepatocyte growth factor receptor (c-met) gene by its ligand (hepatocyte growth factor) is mediated through AP-1. *Oncogene*. 2000;19(9):1132–1137.
7. Jahangiri A, et al. Gene expression profile identifies tyrosine kinase c-Met as a targetable mediator of antiangiogenic therapy resistance. *Clin Cancer Res*. 2013;19(7):1773–1783.
8. Qian LW, et al. Radiation stimulates HGF receptor/c-Met expression that leads to amplifying cellular response to HGF stimulation via upregulated receptor tyrosine phosphorylation and MAP kinase activity in pancreatic cancer cells. *Int J Cancer*. 2003; 104(5):542–549.
9. Engelman JA, Jänne PA. Mechanisms of acquired resistance to epidermal growth factor receptor tyrosine kinase inhibitors in non-small cell lung cancer. *Clin Cancer Res*. 2008;14(10):2895–2899.
10. Lyon M, Deakin JA, Mizuno K, Nakamura T, Gallagher JT. Interaction of hepatocyte growth factor with heparan sulfate. Elucidation of the major heparan sulfate structural determinants. *J Biol Chem*. 1994;269(15):11216–11223.
11. Smolen GA, et al. Amplification of MET may identify a subset of cancers with extreme sensitivity to the selective tyrosine kinase inhibitor PHA-665752. *Proc Natl Acad Sci U S A*. 2006;103(7):2316–2321.
12. Lutterbach B, et al. Lung cancer cell lines harboring MET gene amplification are dependent on Met for growth and survival. *Cancer Res*. 2007; 67(5):2081–2088.
13. Turke AB, et al. Preexistence and clonal selection of MET amplification in EGFR mutant NSCLC. *Cancer Cell*. 2010;17(1):77–88.
14. Linehan WM, et al. Identification of the genes for kidney cancer: opportunity for disease-specific targeted therapeutics. *Clin Cancer Res*. 2007;3(2 pt 2):671s–679s.
15. Michieli P, et al. Mutant Met-mediated transformation is ligand-dependent and can be inhibited by HGF antagonists. *Oncogene*. 1999;18(37):5221–5231.
16. Trusolino L, Comoglio PM. Scatter-factor and semaphorin receptors: cell signalling for invasive growth. *Nat Rev Cancer*. 2002;2(4):289–300.
17. Naldini L, et al. Extracellular proteolytic cleavage by urokinase is required for activation of hepatocyte growth factor/scatter factor. *EMBO J*. 1992; 11(13):4825–4833.
18. Kirchhofer D, et al. Structural and functional basis

research article

of the serine protease-like hepatocyte growth factor β-chain in Met binding and signaling. *J Biol Chem*. 2004;279(38):39915–39924.

19. Matsumoto K, Kataoka H, Date K, Nakamura T. Cooperative interaction between α- and β-chains of hepatocyte growth factor on c-Met receptor confers ligand-induced receptor tyrosine phosphorylation and multiple biological responses. *J Biol Chem*. 1998;273(36):22913–22920.

20. Stamos J, Lazarus RA, Yao X, Kirchhofer D, Wiesmann C. Crystal structure of the HGF β-chain in complex with the Sema domain of the Met receptor. *EMBO J*. 2004;23(12):2325–2335.

21. Merchant M, et al. Monovalent antibody design and mechanism of action of onartuzumab, a MET antagonist with anti-tumor activity as a therapeutic agent. *Proc Natl Acad Sci USA*. 2013;110(32):E2987–E2996.

22. Basilico C, Arnesano A, Galluzzo M, Comoglio PM, Michieli P. A high affinity hepatocyte growth factor-binding site in the immunoglobulin-like region of Met. *J Biol Chem*. 2008;283(30):21267–21277.

23. Yokozaki H. Molecular characteristics of eight gastric cancer cell lines established in Japan. *Pathol Int*. 2000;50(10):767–777.

24. de Haard HJ, et al. Llama antibodies against a lactococcal protein located at the tip of the phage tail prevent phage infection. *J Bacteriol*. 2005; 187(13):4531–4541.

25. de Haard HJ, et al. A large non-immunized human Fab fragment phage library that permits rapid isolation and kinetic analysis of high affinity antibodies. *J Biol Chem*. 1999;274(26):18218–18230.

26. Jin H, et al. MetMAb, the one-armed 5D5 anti-c-Met antibody, inhibits orthotopic pancreatic tumor growth and improves survival. *Cancer Res*. 2008; 68(11):4360–4368.

27. Goetsch L, inventor; Pierre Fabre Medicament, assignee. Antibodies inhibiting c-Met dimerization uses thereof. US patent 20130273060 A1. July 10, 2008.

28. Michieli P, et al. Targeting the tumor and its microenvironment by a dual-function decoy Met receptor. *Cancer Cell*. 2004;6(1):61–73.

29. Pacchiana G, et al. Monovalency unleashes the full therapeutic potential of the DN-30 anti-Met antibody. *J Biol Chem*. 2010;285(46):36149–36157.

30. Martens T, et al. A novel one-armed anti-c-Met antibody inhibits glioblastoma growth in vivo. *Clin Cancer Res*. 2006;12(20 pt 1):6144–6152.

31. Chan GK, Lutterbach BA, Pan BS, Kariv I, Szewczak AA. High-throughput analysis of HGF-stimulated cell scattering. *J Biomol Screen*. 2008;13(9):847–854.

32. Rong S, et al. Tumorigenesis induced by coexpression of human hepatocyte growth factor and the human met protooncogene leads to high levels of expression of the ligand and receptor. *Cell Growth Differ*. 1993;4(7):563–569.

33. Maggiora P, et al. The RON and MET oncogenes are co-expressed in human ovarian carcinomas and cooperate in activating invasiveness. *Exp Cell Res*. 2003;288(2):382–389.

34. Tyan SW, et al. Breast cancer cells induce cancer-associated fibroblasts to secrete hepatocyte growth factor to enhance breast tumorigenesis. *PLoS One*. 2011;6(1):e15313.

35. Mueller KL, Madden JM, Zoratti GL, Kuperwasser C, List K, Boerner JL. Fibroblast-secreted hepatocyte growth factor mediates epidermal growth factor receptor tyrosine kinase inhibitor resistance in triple-negative breast cancers through paracrine activation of Met. *Breast Cancer Res*. 2012;14(4):R104.

36. Kuperwasser C, et al. Reconstruction of functionally normal and malignant human breast tissues in mice. *Proc Natl Acad Sci U S A*. 2004;101(14):4966–4971.

37. De Bacco F, et al. Induction of MET by ionizing radiation and its role in radioresistance and invasive growth of cancer. *J Natl Cancer Inst*. 2011; 103(8):645–661.

38. Galimi F, et al. Genetic and expression analysis of MET, MACC1, and HGF in metastatic colorectal cancer: response to MET inhibition in patient xenografts and pathologic correlations. *Clin Cancer Res*. 2011;17(10):3146–3156.

39. Vermeulen L, et al. Wnt activity defines colon cancer stem cells and is regulated by the microenvironment. *Nat Cell Biol*. 2010;12(5):468–476.

40. Koliaraki V, Roulis M, Kollias G. Tpl2 regulates intestinal myofibroblast HGF release to suppress colitis-associated tumorigenesis. *J Clin Invest*. 2012;

122(11):4231–4242.

41. Céspedes MV, et al. Orthotopic microinjection of human colon cancer cells in nude mice induces tumor foci in all clinically relevant metastatic sites. *Am J Pathol*. 2007;170(3):1077–1085.

42. Niemann HH, et al. Structure of the human receptor tyrosine kinase met in complex with the Listeria invasion protein InlB. *Cell*. 2007;130(2):235–246.

43. Takahashi T, Strittmatter SM. Plexin A1 autoinhibition by the plexin sema domain. *Neuron*. 2001; 29(2):429–439.

44. Prat M, Crepaldi T, Pennacchietti S, Bussolino F, Comoglio PM. Agonistic monoclonal antibodies against the Met receptor dissect the biological responses to HGF. *J Cell Sci*. 1998;111(pt 2):237–247.

45. Rath P, et al. In vivo c-Met pathway inhibition depletes human glioma xenografts of tumor-propagating stem-like cells. *Transl Oncol*. 2013;6(2):104–111.

46. De Bacco F, et al. The MET oncogene is a functional marker of a glioblastoma stem cell subtype. *Cancer Res*. 2012;72(17):4537–4550.

47. Xie Q, et al. Hepatocyte growth factor (HGF) autocrine activation predicts sensitivity to MET inhibition in glioblastoma. *Proc Natl Acad Sci U S A*. 2012; 109(2):570–575.

48. Lefranc F, Brotchi J, Kiss R. Possible future issues in the treatment of glioblastomas: special emphasis on cell migration and the resistance of migrating glioblastoma cells to apoptosis. *J Clin Oncol*. 2005; 23(10):2411–2422.

49. Webb CP, et al. Evidence for a role of Met-HGF/SF during Ras-mediated tumorigenesis/metastasis. *Oncogene*. 1998;17(16):2019–2025.

50. Furge KA, et al. Suppression of Ras-mediated tumorigenicity and metastasis through inhibition of the Met receptor tyrosine kinase. *Proc Natl Acad Sci U S A*. 2001;98(19):10722–10727.

51. de Rock E, Taylor N. An easy method of layering blood over Ficoll-Paque gradients. *J Immunol Methods*. 1977;17(3–4):373–374.

52. Chomczynski P, Sacchi N. Single-step method of RNA isolation by acid guanidinium thiocyanate-phenol-chloroform extraction. *Anal Biochem*. 1987; 162(1):156–159.